Dejana Đorđević

Hydraulic Modelling

The quality of flood risk assessment highly depends on the proper definition of flood hazard maps. The level of confidence of these maps is governed by the quality of the hydrologic and hydraulic models. This course is focused on the hydraulic modelling of floods, i.e. flow in two-stage or compound channels. The course shall provide a state-of-the-art in 1D hydraulic modelling of floods. Models, which take into account different modes of momentum transfer between the main channel and floodplains, lead to better estimation of discharge and, consequently, better design of flood protection measures.

Characteristics of flow structure in compound channels

Overbank flow in a compound channel (CCh), which starts when the conveyance of the main channel is exceeded, is more complex than the inbank flow. The complexity originates from:

1. A sudden expansion of the channel;
2. The presence of vegetation on floodplains as a source of increased roughness when compared to the main channel roughness;
3. A random distribution of vegetation patches; and
4. Meandering of the main channel.

A special working group concerned with flow and sediment transport in compound channels was founded under the auspices of IAHR in the early 1990s aiming at:

1. Studying the characteristics of the overbank (compound channel) flow;
2. Checking a validity of the existing resistance laws that were originally proposed for the inbank flow;
3. Checking a validity of traditional methods for estimation of a stage-discharge curve in a compound channel, such as the single channel method (SCM), which is based on the Chézy-Manning equation that makes use of equivalent roughness coefficient, i.e. weighted roughness over the wetted perimeter, or the divided channel method (DCM) in which the total discharge in the cross-section is estimated as a sum of discharges in subsections with different roughness, again calculated using Chézy-Manning equation;
4. Proposing new methods for stage-discharge curve estimation in a compound channel if needed;
5. Proposing mathematical models of uniform and non-uniform flow in compound channels; and

https://doi.org/10.36250/01052_04

6. Proposing 2D models for description of flow in a cross-section of a compound channel to define velocity and shear-stress distributions across the channel width that are important for the estimation of the transport capacity of the flow and conditions for sedimentation on the floodplains. The research is based on studies of compound channel flow in laboratory flumes, mainly in straight ones of prismatic and non-prismatic type with simple rectangular or trapezoidal subsections (Figure 1). Studies of the overbank flow in the case of meandering main channel are still scarce.

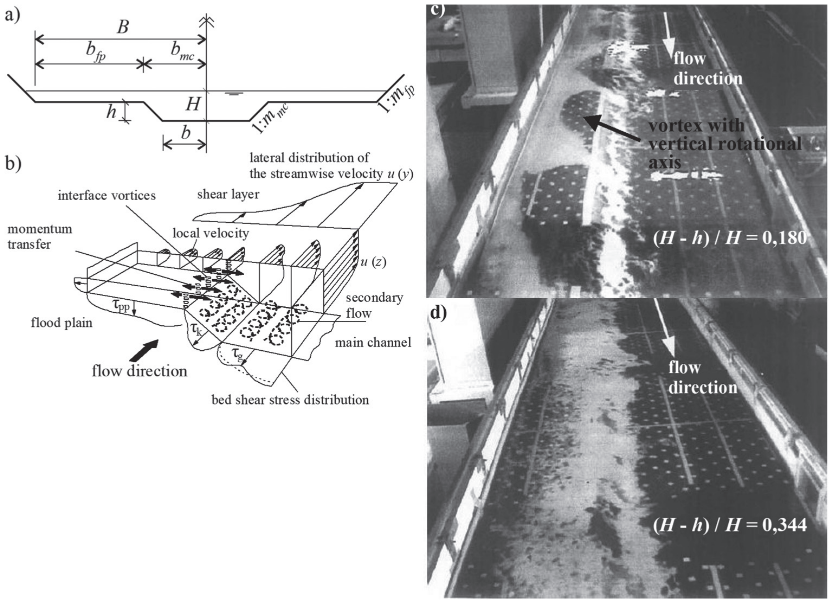

Figure 1. a) Elements of the compound channel geometry; b) flow structure in a compound channel [8]; c) longitudinal vortices with the vertical rotational axis on the floodplain when (H – h) / H = 0.180; and d) shorter longitudinal vortices with the vertical rotational axis on either side of the imaginary boundary between the main channel and the floodplain when (H – h) / H = 0.344 [7]

Experiments in straight prismatic CChs with smooth floodplains have shown that there is an inflection point in the streamwise velocity distribution across the channel width u(y) when the relative depth on the floodplain is low, i.e. when $(H - h) / H < 0.25$ (where H is the flow depth in the main channel and h is the depth of the main channel, Figure 1 a). This type of flow is also called a shallow floodplain flow. Large velocity gradients caused by the difference between the fast flow in the main channel and the slow flow over the floodplain result in increased shear between the two flows and the so-called Kelvin-Helmholz instability. This further gives rise to the development of large clockwise rotating horizontal (planform) vortices along the interface between the main channel and the floodplain on the floodplain side (Figure 1 c). These vortices are responsible for the momentum exchange between the main channel and floodplain flows and additional head losses. The exchange of momentum is accomplished by the turbulence diffusion

$\overline{u'v'}$ on the horizontal and $\overline{u'w'}$ vertical planes (Figure 1 b). With the increase in relative depth on the floodplain [$(H - h) / H > 0.25$], i.e. when the flow on the floodplain turns to a deep floodplain flow, the u-velocity becomes more evenly distributed across the channel width and the inflection point turns to a velocity dip. Thus, there are velocity gradients on both sides of the interface between the main channel and the floodplain. They give rise to the development of two counter rotating planform vortices on each side of the interface. These vortices are much smaller than those that develop in shallow floodplain flow (Figure 1 d), because of the strong secondary flow at the junction of the main channel and the floodplain, which now governs the 3D flow structure in CCh, as found by Nezu et al. and Ikeda et al. [8].

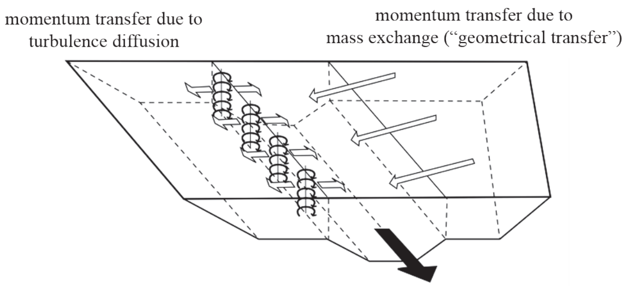

Figure 2. Types of momentum transfer between the main channel and floodplains [5]

The 3D flow in straight non-prismatic channels is further enhanced due to increased overflow from the main channel to the floodplains in case of a CCh with the diverging floodplains or due to inflow of water from the floodplains to the main channel in case of converging floodplains.

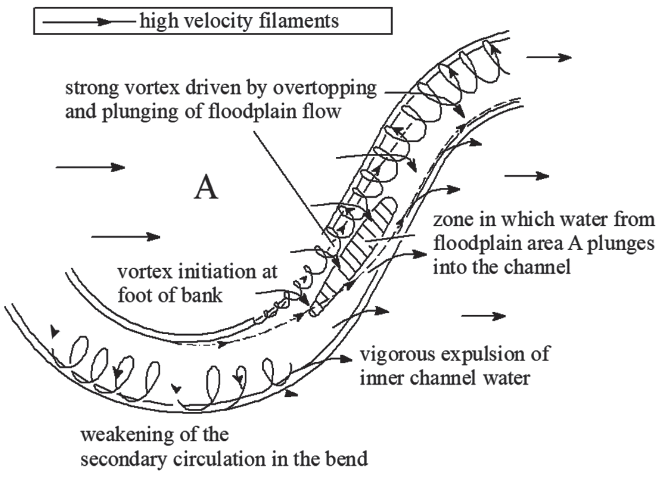

Figure 3. Interaction between the flow down the valley and the flow in the main channel in case of meandering channels [8]

This gives rise to additional momentum exchange between the two subsections of the CCh due to mass exchange, the so-called “geometrical transfer” (Figure 2). The total momentum transfer is thus the sum of the two components. Both components are lateral momentum exchanges between the two alongside flows. When the main channel meanders, there is also an interaction between the flow down the valley and that in the main channel (Figure 3). However, this type of flow has not yet been sufficiently investigated.

Despite of the fact that Prof. Miodrag Radojković from the Faculty of Civil Engineering in Belgrade suggested first improvements of the traditional procedure for calculation of 1D uniform and non-uniform flows in two-stage (CCh) channels in the mid-1980s, the DCM is still used by the vast majority of hydraulic engineering community. The suggested improvement was based on the analysis of forces that act on the three main subsections of the CCh, when they are observed independently, i.e. on the main channel and the two floodplains. The essence of Radojković’s approach rests in the inclusion of the momentum transfer between the main channel and the floodplains via so-called ϕ-index, which is the ratio of the shear force and the component of the gravity force that acts in the flow direction in each of the three CCh subsections [16]. The ϕ-index method was successfully used by the working group members in processing of the data from the main flood channel facility at HR Wallingford. Moreover, Wormleaton and Merrett have shown that the method is equally applicable to different types of CCh division into subsections as presented in Figure 4, and that the best fit with measurements is achieved for rough floodplains when the interaction between the main channel and floodplain flows is pronounced.

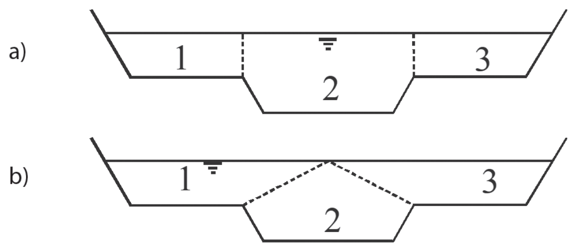

Figure 4. Possible divisions of the compound channel into subsections in the DCM; a) division using vertical; b) diagonal plains [16]

Ackers [1] proposed an empirical procedure for the improvement of the DCM results based on a large amount of experimental data a few years later. The essence of this approach is in calculation of the coherence, i.e. the ratio of the conveyance of the cross-section as a single unit and the sum of segment conveyances. Thus, coherence is a non-dimensional parameter and an indicator of the hydraulic homogeneity of the cross-section of the CCh. The discharge values calculated using the coherence method are less than those obtained by the DCM, but larger than values calculated using the SCM [8] [4].

Bousmar and Zech [2] proposed a physically based 1D mathematical model of uniform/non-uniform flow in a CCh in the late 1990s – an exchange discharge model (EDM).

Apart from losses due to friction, the energy losses in this method also include those originating from the momentum exchange between the main channel and floodplains. As already mentioned, there are two principal sources of the exchange of momentum. These are turbulent diffusion and mass exchange or "geometrical transfer". The EDM model, as shown by [1] and [4] provides much better agreement with measured stage-discharge curves than Ackers's method and the two traditional methods – SCM and DCM. Later on, in the early 2000s Proust et al. [12] improved the 1D mathematical model of non-uniform flow in a CCh proposed by Yen et al., and named it "independent subsections method" (ISM). Both the mass and momentum conservation equations are written for each subsection of the CCh as in the EDM. However, the main difference is in the numerical procedure used to solve these equations. While all equations in the EDM are combined in a single non-linear equation with one unknown variable, which is solved using the Newton-Raphson method, the system of equations is kept together in the ISM and solved iteratively using the finite difference method. Energy losses due to turbulent and mass exchanges are calculated in a similar fashion as in the EDM.

The role of vegetation, its effect on flow structure and its environmental effect

Until recently, vegetation was considered only a source of flow resistance. Therefore, it was frequently removed from channels and floodplains to enhance flow conveyance and reduce flooding. However, it was gradually recognised (during the last twenty years) that vegetation also provides a wide range of ecosystem services, such as: 1. The uptake of nutrients (nitrogen and phosphorous); 2. The production of oxygen; 3. The promotion of biodiversity by creation of spatial heterogeneity in stream velocity; 4. The attenuation of waves on the water surface; 5. The enhancement of bank stability; and 6. Trapping of sediment particles. This wide range of ecosystem services results from the fact that the vegetation alters the velocity field across different scales, which range from individual blades and branches of a single plant, to a community of plants in a meadow or a patch. Having this in mind, the proper description of the physical role of vegetation in the environment requires identification of the spatial scale relevant to a particular process. Thus, a brief review of flow structures starting from the blade scale, via patch scale to the reach scale will be highlighted in this section.

Vegetation can be emergent, when the flow depth is below its crest, or submerged, when there is a layer of water above its crest. Either one can be rigid or flexible.

Blade and individual stem scale

Flow around individual blades and leaves is modelled using the flat plate boundary-layer (Figure 5). The thickness of a viscous boundary layer, that forms at the leading edge (x = 0) of a plate, gradually grows in the streamwise direction $\delta(x) = 5\sqrt{\nu x / U}$. The viscous layer becomes sensitive to perturbations in the outer flow with the increasing thickness. When Reynolds number $R_x = U\,x / \nu$ approaches the value of 10^5, a transition to the turbulent boundary layer with the viscous sub-layer δ_s close to the blade surface occurs. Two possible cases are distinguished: one, in which the blade length is less than the transition length, and the other, in which the boundary layer becomes turbulent over a considerable portion of the blade length. In the first case, the boundary layer is laminar over the entire blade. In the latter one, the viscous sub-layer will have a constant thickness set by the friction velocity on the blade u_{b*}.

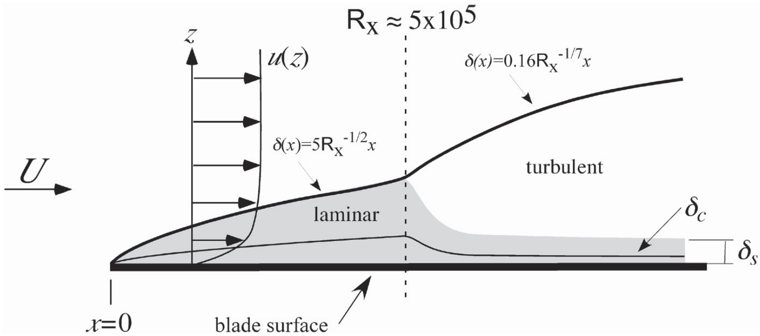

Figure 5. A flat plate boundary-layer model. The momentum boundary layer, δ, grows with distance from the leading edge (x = 0). Initially, the boundary layer is laminar (shaded grey). At distance x, corresponding to $R_x = xU/\nu \approx 5 \times 10^5$, the boundary layer becomes turbulent, except for a thin layer near the surface that remains laminar, called the viscous (or laminar) sub-layer, δ_s. In water, the diffusive sub-layer, δ_c, is much smaller than the viscous sub-layer, with $\delta_c = \delta_s S^{-1/3}$, where $S = \nu/D_m$ is the Schmidt number. The vertical coordinate is exaggerated in this figure [10]

The viscous sub-layer thickness is between $\delta_s = 5\nu/u_{b*}$ and $10\nu/u_{b*}$. Within this layer, the flow is essentially laminar. In addition to the viscous sub-layer, there is the concentration boundary layer δ_c. The thickness of this layer is smaller than δ_s ($\delta_c = 0.1\delta_s$), because of the difference in magnitude between the molecular diffusivity (D_m), whose order is 10^{-9} m²/s, and molecular viscosity, i.e. kinematic viscosity of water ν, which is of the order 10^{-6} m²/s.

Plants can have rigid and flexible stems. Flexible plants can be pushed over by currents, resulting in a change in morphology called reconfiguration [10]. Reconfiguration reduces flow resistance via two mechanisms: the reduction of the frontal area and the streamline adjustment. The drag on the deflected stem increases more slowly with velocity than that predicted by the quadratic law [10]. Recent studies have shown that reconfiguration depends on two dimensionless parameters, namely the Cauchy number and the buoyancy parameter. The Cauchy number (C) is the ratio of drag to the restoring force due to rigidity, while the buoyancy parameter (B), is the ratio of the restoring forces due to buoyancy and stiffness. For a stem of height *h*, width *w*, thickness *t*, and density, ρ*v*, the two parameters are defined in a uniform flow of horizontal velocity *U* as:

$$C = \frac{1}{2}\frac{\rho C_D w U^2 h^3}{EI} \tag{1}$$

$$B = \frac{(\rho - \rho_v) g w t h^3}{EI} \tag{2}$$

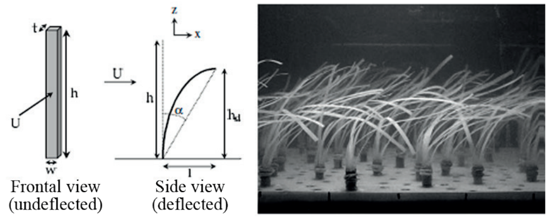

Figure 6. Geometric characteristics of individual undeflected and deflected stems (left) and a photograph from the experiments of Ghisalberti and Nepf [6]

In these expressions, E is the elastic modulus for the stem, I (= wt^3 /12) is the second moment of area, ρ is the density of water and g is the acceleration due to gravity.

The impact of reconfiguration on drag can be described by an effective blade height (h_e) which is defined as the height of a rigid, vertical stem that generates the same horizontal drag as a flexible one of total height h [10]. Based on this definition, the horizontal drag force is $F_x = (1/2)\rho C_D w h e U^2$, where the drag coefficient C_D is identical to that of rigid, vertical stems. The following relationships for effective height (h_e) and meadow height (h_m), are based on the model described in Luhar and Nepf [10]:

$$\frac{h_e}{h} = 1 - \frac{1 - 0.9\,C^{-1/3}}{1 + C^{-3/2}\,(8 + B^{3/2})} \tag{3}$$

$$\frac{h_m}{h} = 1 - \frac{1 - 0.9\,C^{-1/4}}{1 + C^{-3/5}\,(4 + B^{3/5}) + C^{-2}\,(8 + B^2)} \tag{4}$$

When rigidity is the dominant restoring force (C>>B), Eq. 4 reduces to $h_m / h \sim C^{-1/4} \sim (EI/U^2)^{1/4}$ [10].

Patch scale

Uniform meadows of submerged vegetation are communities of individual plants of different densities. The meadow geometry is defined by the size of individual stems and their number per bed area. The meadow density can be defined in three different ways: 1. as the frontal area per volume $a = d / \Delta S^2$ (where d is a characteristic diameter or width and ΔS is an average spacing between stems); 2. as the solid volume fraction occupied by the canopy elements ϕ; or 3. as the frontal area per bed area $\lambda = ah_m$, which is known as a roughness density. Due to spatial heterogeneity of the velocity field, the flow in submerged meadows is described using the double-averaging concept proposed by Nikora et al. [11]. The length scale over which both mean and turbulent velocity components adjust to canopy drag is known as the canopy-drag length scale. This length scale is defined as:

$$L_c = \frac{2\,(1-\phi)}{C_D\, a} \tag{5}$$

and the spatially-averaged meadow drag as:

$$D_x = \frac{1}{2}\,\frac{C_D\, a}{(1-\phi)}\,\langle \overline{u} \rangle \left| \langle \overline{u} \rangle \right| \tag{6}$$

Here operator$\langle\ \rangle$stands for spatial averaging explained in Nikora et al. [11]. “The effect of meadow density, expressed via roughness density, on the velocity profiles and turbulence scales is presented in Figure 7. Two limits of flow behaviour are distinguished depending on the relative importance of the bed shear and meadow drag. If the meadow drag is smaller than the bed drag, then the velocity follows a turbulent boundary-layer profile, with the vegetation contributing to the bed roughness. This is the sparse canopy limit (Figure 7 a). In this limit, the turbulence near the bed will increase as stem density increases. Alternatively, in the dense canopy limit, the canopy drag is larger than the bed stress, and the discontinuity in drag at the top of the canopy generates a region of shear resembling a free shear layer, including an inflection point near the top of the canopy (Figure 7 b, c). From scaling arguments, the transition between sparse and dense limits occurs at $\lambda = ah_m = 0.1$. From measured velocity profiles, a boundary-layer form with no inflection point is observed for $C_D ah_m < 0.04$, and a pronounced inflection point appears for $C_D ah_m > 0.1$” [10].

“If the velocity profile contains an inflection point, it is unstable to the generation of Kelvin–Helmholtz (KH). These structures dominate the vertical transport at the canopy interface. These vortices are called canopy-scale turbulence, to distinguish them from the much larger boundary-layer turbulence, which may form above a deeply submerged or unconfined canopy, and the much smaller stem-scale turbulence. Over a deeply submerged (or terrestrial) canopy ($H / h > 10$), the canopy-scale vortices are highly three dimensional due to their interaction with boundary-layer turbulence, which stretches the canopy-scale vortices, enhancing secondary instabilities. However, with shallow submergence ($H / h \leq 5$), which is common in aquatic systems, large-scale boundary-layer turbulence is not developed, and the canopy-scale vortices dominate the turbulence both within and above the meadow” [10].

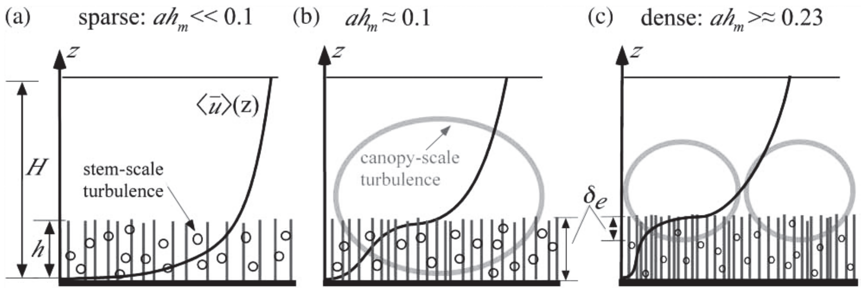

Figure 7. The mean velocity profiles through submerged meadows of increasing roughness density (ah_m). The meadow height is hm. Water depth is H. a) For ah_m < 0.1 (sparse regime), the velocity follows a rough boundary-layer profile; b) for $ah_m \geq 0.1$, a region of strong shear at the top of the canopy generates canopy-scale turbulence. The canopy-scale turbulence penetrates a distance δ_e = [0.23 ± 0.06]($C_D a$) −1 into the canopy; c) for ah_m > 0.23 (dense regime), δ_e < h, and the bed is shielded from the canopy-scale turbulence. Stem-scale turbulence is generated throughout the meadow [10]

"Within a distance of about $10h_m$ from the canopy's leading edge, the canopy-scale vortices reach a fixed scale and a fixed penetration into the canopy. The final vortex and shear-layer scale is reached when the shear production that feeds energy into the canopy-scale vortices is balanced by the dissipation by the canopy drag. This balance predicts the following scaling, which has been verified with observations" [10]:

$$\delta_e = \frac{0.23 \pm 0.6}{C_D a} \tag{7}$$

"This equation only applies to canopies that form a shear layer (i.e. $C_D a h_m \geq 0.1$). For $C_D a h_m$ = 0.1–0.23, the canopy-scale turbulence penetrates to the bed, $\delta_e = h_m$, creating a highly turbulent condition over the entire canopy height (Figure 7 b). At higher values of $C_D a h_m$, the canopy-scale turbulence does not penetrate to the bed, $\delta_e < h_m$ (Figure 7 c). If the submergence ratio $H / h_m < 2$, E_q. 7 for δ_e is not applicable, as the interaction with the water surface diminishes the strength and size of the canopy-scale vortices. Canopies for which $\delta_e / h_m < 1$ (Figure 7 c) shield the bed from strong turbulence and turbulent stress. Because turbulence near the bed plays a role in resuspension, these dense canopies are expected to reduce re-suspension and erosion" [10].

Long patches of emergent canopies of finite width can grow either along the bank (Figure 8) or may exist at the centre of a channel (Figure 9). The width of alongside canopies is denoted by *b*. In case of centreline canopies, *b* is half the width of the canopy strip. The approaching flow deflects upstream of the patch due to high drag exerted by vegetation. The upstream distance over which deflection starts is set by the scale *b* and it continues a distance x_D into the vegetation. The shear layer with KH vortices develops along the lateral edge of vegetation only after the deflection is complete ($x > x_D$). The initial growth, the final scale of the horizontal shear layer vortices and their lateral penetration into the patch δ_L, are depicted in Figure 8. The vortices extend into the open channel over length $\delta_0 \sim H/C_f$, where C_f is the bed friction [10]. There is no direct relation between δ_L and δ_0. The penetration depth is defined as:

$$\delta_L = \frac{0.5 \pm 0.1}{C_D a} \tag{8}$$

“If the patch width, b, is greater than the penetration distance, δ_L ($C_D ab > 0.5$, according to Eq. 8), turbulent stress does not penetrate to the centreline of the patch and the velocity within the patch (U_1, Figure 8) is set by a balance of potential gradient (bed and/or water surface slope) and vegetation drag. In contrast, for $C_D ab < 0.5$, turbulence stress can reach the patch centreline, and U_1 is set by the balance of turbulence stress and vegetation drag.

The centre of each vortex is a point of low pressure, which, for shallow flows, induces a wave response across the entire patch and specifically beyond δ_L from the edge. The wave response within the vegetation has been shown to enhance the lateral (y) transport of suspended particles, above that predicted from stem turbulence alone. For in-channel patches, shear layers develop along both flow parallel edges, and the vortices along each edge interact across the canopy width (Figure 9 a). The low-pressure core associated with each vortex produces a local depression in the water surface, such that the passage of individual vortices can be recorded by a surface displacement gage. A time record of surface displacement measured on opposite sides of a patch (A1 and A2 in Figure 9 b) shows that there is a half-cycle phase shift (π radians) between the vortex streets that form on either side of the patch. Because the vortices are a half cycle out of phase, when the pressure (surface elevation) is at a minimum on side A1, it is at a maximum at side A2. The resulting cross-canopy pressure gradient induces a transverse velocity within the canopy (Figure 9 b) that lags the lateral pressure gradient by π/2, that is, a quarter cycle. The synchronisation of the vortex streets occurs even when the vortex penetration is less than the patch width, $\delta_L / b < 1$, and it significantly enhances the vortex strength and the turbulence momentum exchange between the open channel and vegetation. More importantly, the vortex interaction introduces significant lateral transport across the patch” [10].

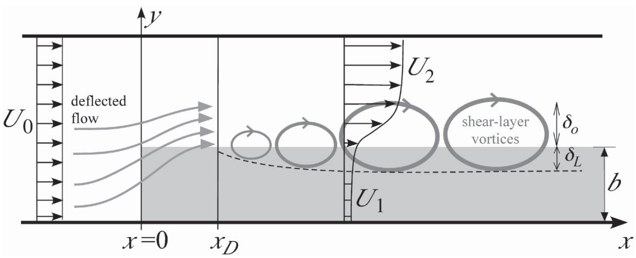

Figure 8. Top view of a channel with a long patch of emergent vegetation along the right bank (grey shading). The width of the vegetated zone is b. The flow approaching from upstream has uniform velocity U_0. The flow begins to deflect away from the patch at a distance b upstream and continues to decelerate and deflect until distance x_D. After this point, a shear layer forms on the flow-parallel edge and shear-layer vortices form by KH instability. These vortices grow downstream, but subsequently reach a fixed width and fixed penetration distance into the vegetation, δ_L [10].

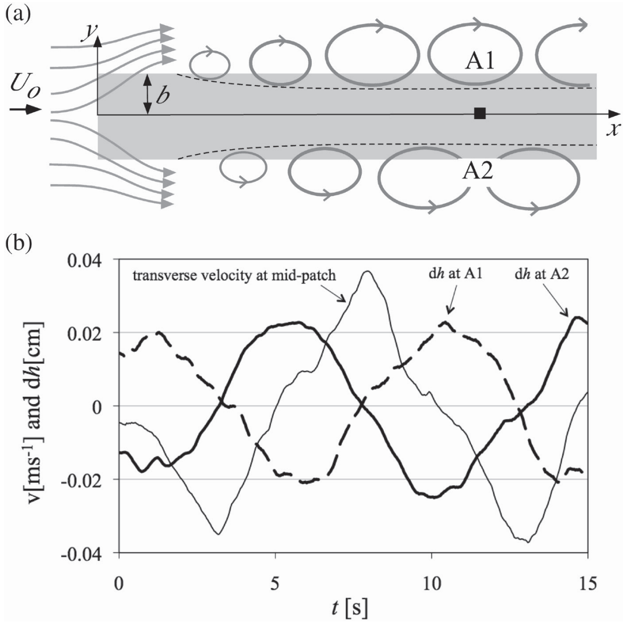

Figure 9. a) Top view of emergent vegetation with two flow-parallel edges. The patch width is 2b. The coherent structures on either side of the patch are out of phase. The passage of each vortex core is associated with a depression in surface elevation, which is measured at the patch edges (A1 and A2). The velocity is measured mid-patch (square). b) Data measured for a patch of width b = 10 cm in a channel with flow velocity U_0 = 10 cm s^{-1}. The patch centreline velocity is U_1 = 0.5 cm s^{-1}. The surface displacements measured at A1 (heavy dashed line) and at A2 (heavy solid line) are a half cycle (π radians) out of phase. The resulting transverse pressure gradient imposed across the patch generates transverse velocity within the patch (thin line), which, as in a progressive wave, lags the lateral pressure gradient by a quarter cycle (π/2 radians) [10].

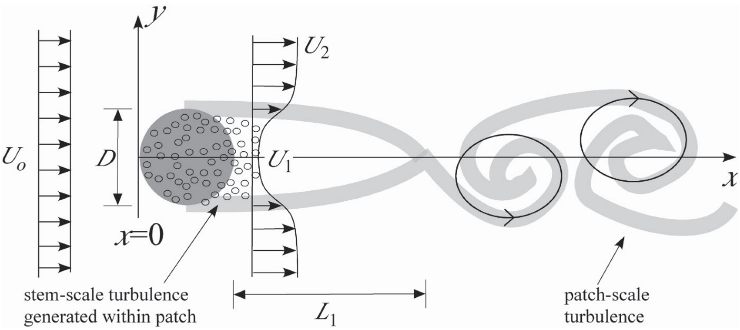

Figure 10. Top view of a circular patch of emergent vegetation with patch diameter D. The upstream, open-channel velocity is U_0. Stem-scale turbulence is generated within the patch, but dies out quickly behind the patch. The flow coming through the patch (U_1) blocks interaction between the shear layers at the two edges of the patch, which delays the onset of the patch-scale vortex street by a distance L_1. Tracer (grey line) released from the outermost edges of the patch comes together at a distance L_1 downstream from the patch and reveals the von Karman vortex street [10]

Circular patch of emergent vegetation

A circular patch with diameter D (Figure 10) is used as a model. "Because the patch is porous, the flow passes through it, and this alters the wake structure relative to that of a solid body. Directly behind a solid body, there is a region of recirculation, followed by a von Karman vortex street. The wake scale mixing provided by the von Karman vortices allows the velocity in the wake to quickly return (within a few diameters) to a velocity comparable to the upstream velocity (U_0). In contrast, the wake behind a porous obstruction (patch of vegetation) is much longer, because the flow entering the wake through the patch (called the bleed flow) delays the onset of the von Karman vortex street until a distance L_1 behind the patch. As a result, the velocity at the centreline of the wake, U_1, remains nearly constant over distance L_1. Within this region, both the velocity and turbulence are reduced, relative to the adjacent bare bed, so that it is a region where deposition is likely to be enhanced.

Both U_1 and L_1 depend on the patch diameter, D, and the drag length scale, $L_c \sim (C_D a)^{-1}$, which together form a dimensionless parameter, $C_D aD$, called the flow blockage. For low flow blockage (small $C_D aD$), U_1/U_0 decreases linearly with $C_D aD$. Using $C_D = 1$, a reasonable linear fit is:

$$\frac{U_1}{U_0} = 1 - [0.33 + 0.08] C_D \, a D \tag{9}$$

For high flow blockage, U_1 is negligibly small ($U_1 / U_\infty \approx 0.03$), but not zero. However, at some point around $C_D aD = 10$, U_1 does become zero, and the flow field around the porous patch becomes identical to that around a solid obstruction. This transition is also seen in the length scale, L_1, discussed below. Zong and Nepf suggested that L_1 may be predicted from the linear growth of the shear layers located on either side of the near-wake region, from which they derived:

$$\frac{L_1}{D} = \frac{1}{4S_1} \frac{(1 + U_1/U_0)}{(1 - U_1/U_0)} \tag{10}$$

Where S_1 is a constant (0.10 ± 0.02) across a wide range of D and ϕ. Drag is produced at two distinct scales: the leaf and stem scale and the patch scale. For low flow blockage patches, there is sufficient flow through the patch that the stem and leaf-scale drag dominates the flow resistance, that is, the flow resistance can be represented by the integral of $C_D au^2$ over the patch interior, with u being the velocity within the patch. However, for high flow-blockage patches, there is negligible flow through the patch, and the integral of $C_D au^2$ over the patch interior is irrelevant. The flow response to a high flow-blockage patch is essentially identical to the flow response to a solid obstruction of the same patch frontal area, A_p. Thus, the flow resistance provided by the patch should be represented by the patch-scale geometry, that is, $C_D A_p U^2$, with U being the channel velocity. This idea is supported by measurements of flow resistance produced by sparsely distributed bushes. A bush consists of a distribution of stems and leaves and so is a form of vegetation patch. The flow resistance generated by the bushes fit the quadratic model, ρ $C_D A_p U^2$, and notably C_D was $o(1)$, similar to a solid body. Thus, although porous, the bush generated drag that was comparable to that of a solid object of the same size (A_p). It is worth noting that C_D decreased somewhat (from 1.2 to 0.8) as the channel velocity increased. This shift is most likely due to the reconfiguration of stems and leaves that reduced A_p" [10].

Reach scale

"At the scale of the channel reach, flow resistance due to vegetation is determined primarily by the blockage factor (B_x) which is the fraction of the channel cross-section blocked by vegetation. For a patch of height h_m and width w in a channel of width W and depth H, $B_x = wh / WH$. Different studies show strong correlations between B_x and Manning's roughness coefficient n_M, noting that the relationship is nonlinear. For vegetation that fills the channel width, $B_x = h_m / H$. A few studies suggest that the vegetation distribution may also influence the resistance and specifically that greater resistance is produced by distributions with a greater interfacial area between vegetated and non-vegetated regions" [10]. Some authors have "quantified the impact of interfacial area by considering channels with the same blockage factor (B_x), but a different number (N) of patches. They showed that for realistic values of N, the resistance is increased by at most 20%, so that $N = 1$ is a reasonable simplifying assumption. For $N = 1$, the momentum balance leads to the following equations for Manning's roughness" [10]:

$$\text{For } B_x = 1: \qquad n_M \left(\frac{g^{1/2}}{K H^{1/6}} \right) = \left(\frac{C_D a H}{2} \right)^{1/2} \tag{11}$$

$$\text{For } B_x < 1: \qquad n_M \left(\frac{g^{1/2}}{K H^{1/6}} \right) = \left(\frac{C_*}{2} \right)^{1/2} (1 - B_x)^{-3/2} \tag{12}$$

"The constant $K = 1\ \text{m}^{1/3}\ \text{s}^{-1}$ is required to make the equations dimensionally correct. Note that Eq. 11 is valid when $B_x = 1$, which indicates that vegetation covers the entire cross-section, width and depth. The coefficient C_* parameterises the shear stress at the interface between vegetated and non-vegetated regions, and $C_* = 0.05$–0.13, based on fits to field data, as shown by Luhar and Nepf. For the case of submerged vegetation that fills the channel width, the resistance is a function only of the submergence depth (H / h_M). Here, an expression for Manning's coefficient, proposed by Luhar and Nepf is presented:

$$\text{For } H/h > 1: \qquad n_M \left(\frac{g^{1/2}}{K H^{1/6}} \right) = \left[\left(\frac{2}{C_*} \right)^{1/2} \left(1 - \frac{h}{H} \right)^{3/2} + \left(\frac{2}{C_D a h_M} \right)^{1/2} \frac{h_M}{H} \right]^{-1} \tag{13}$$

If $C_D a h_M > C_*$, a common field condition, the second term drops out and Eq. 13 reverts to Eq. 12, because $B_x = h_M / H$ for vegetation covering the full channel width [10].

Floodplain processes

Floodplain processes are associated with the overbank deposition of sediment from river channels and overbank flow. As far as the deposition of sediments is concerned, two major mechanisms are distinguished: 1. The deposition due to interaction with the main channel; and 2. The deposition around vegetation. The deposition has important implications for floodplain development, agriculture and environment due to accumulation of contaminants that are adsorbed to sediment particles and for the creation of future sediment sources for the river channel [13]. The transfer of suspended sediment to, and its deposition on the floodplain are affected by the interaction of channel and overbank flows. This interaction, as it was shown in the second section varies with the channel planform. Thus, it may similarly be expected that the deposition pattern varies with the planform. This further means that the deposition pattern may be altered by channel engineering, for example, through channel straightening or through returning previously straightened channels to a more natural meandering state [15].

Floodplain deposition due to interaction with main channel

Intensive turbulent mixing in a lateral direction, which results from the interaction between the main channel and floodplain flows, or between the free flow and that in the vegetation zone, causes lateral net transport of suspended sediment from the main channel flow to the floodplain or the vegetated zone. Consequently, sediment ridges are developed on the floodplain or around the vegetated zone even in straight CChs. The entrainment and longitudinal transport of sediments from the bed are intensified in the main channel during floods, while the transport over the floodplain and through the vegetation is comparably low. This gives rise to the difference in sediment concentration between the main channel and the floodplain or vegetated zone and affects lateral diffusion of sediments.

Although the interaction between the main channel flow and the floodplain results in complex, three-dimensional flow structure (Figure 1 a), the presence of emergent vegetation makes flow horizontally two-dimensional. Such a flow is accompanied with organised fluctuations of low frequency that are caused by KH instability of the horizontal shear flow. They are felt throughout the flow depth and cause fluctuations in bed-load direction. These fluctuations are responsible for the net lateral transport of bed-load from the main channel, where the bed-load concentration is higher, towards the vegetated zone, where the concentration is lower. Thus, a longitudinal ridge is formed on the shoreline near the vegetated zone.

Floodplain deposition around vegetation

When the floodplain is dry, vegetation often forms colonies (Figure 11). It was shown in the previous section that the free flow (the overbank flow in this case) is retarded through and around an isolated vegetated area and that it accelerates again downstream of the vegetation patch to recover velocity. The resulting effect is arrestment of fine sediments and their deposition inside and downstream of the vegetation patch. The accumulated fertile soil facilitates invasion of new vegetation after the flood is retarded. Consequently, the vegetated area is enlarged and spread downstream. Transfer of bed-load from the main channel with the intense overbank flow during major flood events causes development of bed load deposits upstream of the vegetated area (with some local scour just in front of the vegetation) and erosion of its sides. As a result, the vegetated area resembles a mound [15]. The vegetation then becomes more firmly established and the vegetated mound is enlarged in the longitudinal direction, thus changing the morphology of the floodplain (Figure 11).

Figure 11. Vegetation colony on a floodplain [15]

Additionally, a smaller bed shear stress at the floodplains induces deposition of fine sediment on the floodplains.

Floodplain processes by overbank flow

A compound channel consists of a main channel and floodplains between the channel and levees. Floodplains contain many interesting micro-morphological features such as: secondary channels, side pools, dead zones, and so on. They are sometimes associated with vegetation, and vegetation influences fluvial processes related to these morphological features [15]. Furthermore, the variety of micro-morphological features provides favourable habitats for many organisms which contribute to the fluvial ecosystem. As with the original floodplain which existed before construction of levees, these morphologies are exposed to cyclical wetting and drying and cyclical development and destruction.

A typical morphological process which takes place when the overbank flow returns to the main channel is gully head-cutting. Gully head-cutting is characteristic for meandering compound channels or straight channels with alternate bars. This is a retrogressive erosion process, i.e. it migrates upstream. The flow from the gully is concentrated and forms an impinging jet which makes a scour hole (Figure 12). When the scour hole is deep enough, the upstream slope falls down into the scour hole, and the head-cut head migrates upstream.

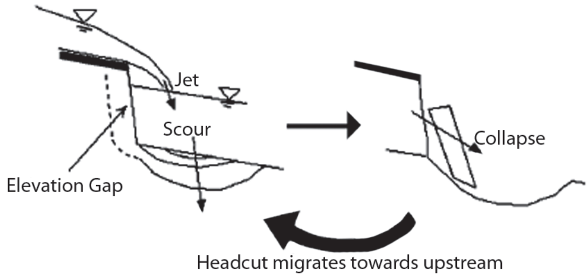

Figure 12. Head-cut erosion [15]

Overview of 1D models for compound channel flow modelling

Exchange discharge model (EDM)

The derivation of the governing equations in the EDM is based on the division of the compound channel cross-section into subsections with uniform hydraulic roughness using vertical planes (Figure 4 a). Generally, there are three subsections: the main channel and two floodplains. With this division, each subsection acts as a channel submitted to lateral flow per unit length of the interface between adjacent subsections q_l (Figure 13). This lateral flow has two components – an inflow q_{in} and an outflow q_{out}. With this decomposition, the mass conservation equation for each subsection can be written as follows:

$$\frac{\partial A}{\partial t}+\frac{\partial Q}{\partial t}=q_l=q_{in}-q_{out} \tag{14}$$

Here the subscript i, indicating the subsection number (i = 1, 2, 3) is omitted for brevity. The space coordinate in the flow direction x and the time t are independent variables, while the cross-sectional area A, the flow discharge Q and the lateral discharge q_l are dependent variables. The two lateral flow components (q_{in} and q_{out}) are mutually exclusive only in prismatic channels. However, this is not the case with the momentum transfer due to turbulence diffusion, as will be shown shortly.

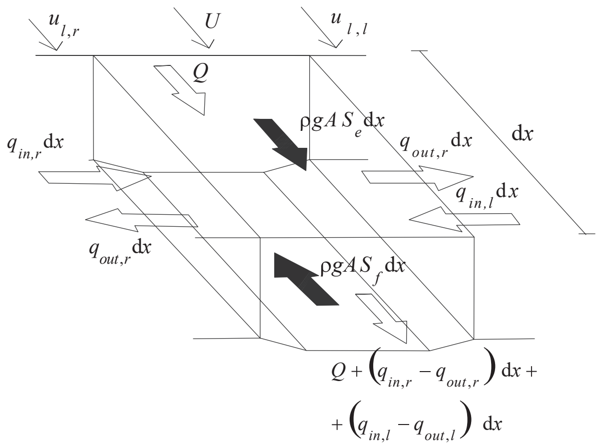

Figure 13. Momentum equilibrium for the control volume in the main channel [2] [4]

The change in the rate of momentum flux through the boundary of a control volume, caused by the action of forces, leads, according to the principle of conservation of momentum to the change in the rate of accumulation of momentum within this volume. Thus, the momentum conservation equation for the control volume of infinitesimal length dx (Figure 13) reads:

$$\frac{\partial}{\partial t}(\rho A U) + \frac{\partial}{\partial x}\left(\rho A U^2\right) + \rho g A \frac{\partial Z}{\partial x} + \rho g A S_f - \rho q_{in} u_l + \rho q_{out} U = 0 \tag{15}$$

The subscript i, indicating the subsection number ($i = 1, 2, 3$) is omitted here for brevity, again. In the previous equation r is the density of water, $U = Q / A$ is the mean velocity in the considered subsection, Z is the water level in the compound channel cross-section, g is acceleration due to gravity, S_f is the slope of the energy grade line, and u_l is the velocity of the lateral inflow in the direction of the main flow. As can be seen, the difference in mean velocities in adjacent subsections of the compound channel cross-section leads to different conveyances of momentum by the inflow and outflow lateral discharges. After the division of Eq. 15 with ρ the application of the product derivative rule, and utilisation of the mass conservation equation 1, the previous equation is simplified to:

$$A\frac{\partial U}{\partial t} + gA\frac{\partial}{\partial x}\left(Z + \frac{U^2}{2g}\right) = q_{in}\left(u_l - U\right) - gAS_f \tag{16}$$

The equation shows that only lateral inflow (q_{in}) affects momentum transfer, while the effect of the outflow is implicitly included in the variation of the kinetic energy head (the second term on the left hand side) [2]. An important consequence of this imbalance in the inflow and the outflow is the transfer of momentum due to turbulence diffusion, even when the average mass transfer through the interface between adjacent subsections is equal to zero (which is the case in prismatic compound channels).

The first term on the left hand side vanishes when the flow is steady. Thus, Eq. 16 simplifies to:

$$S_e = -\frac{\partial}{\partial x}\left(Z+\frac{U^2}{2g}\right) = S_f + \frac{q_{in}\left(U-u_l\right)}{gA} \tag{17}$$

which is the energy conservation equation for steady flow. The S_e is the total head loss per unit length. It is readily noticeable form this equation that the mechanical energy of the compound channel flow is extracted both by the friction and the exchange of discharges at the interface between adjacent subsections. The second term on the right hand side defines additional head loss per unit length due to exchange in discharges, and it will be denoted as S_{mot}. Generally, there are two adjacent subsections. Thus, the lateral inflow can be presented as a sum inflow from the right and the left subsections. Eq. 17 can now be written as:

$$S_e = S_f + \frac{q_{in,r}\,(U-u_{l,r}) + q_{in,l}\,(U-u_{l,l})}{gA} = S_f + S_{mot} \tag{18}$$

To facilitate further derivation of the model, a ratio between the additional loss due to momentum transfer and the friction loss $\chi = S_{mot} / S_f$ is introduced, and the previous equation simplifies to:

$$S_e = S_f\,(1+\chi) \tag{19}$$

It is very important here to note that the total energy slope S_e is unique for the cross-section of the compound channel as a whole, while slopes due to friction S_f and momentum transfer S_{mot} may differ in each subsection because of the difference in roughness in the main channel and on the floodplains. Therefore, these slopes will be defined for each subsection i: $S_{f,i}$ and $S_{mot,i}$, as well as their ratio χ_i, $i = 1, 2, 3$.

The total lateral flow q_l, or exchange discharge, can be divided into two parts – one that is related to the turbulent momentum flux (q^t_{in}) and the other, which is associated to the mass exchange caused by non-prismatic shape of the compound channel (q^g_{in}). The two components should be modelled to close the problem.

Turbulence momentum flux modelling

This term is modelled by using the mixing length model on a horizontal plane. Bousmar and Zech have chosen this model as it allows for relatively simple computational procedure for the estimation of the stage-discharge curve and the definition of the relationship between the discharge and the slope of the energy grade line [2].

The lateral outflow from the main channel to the floodplain q^t_{mfp} and the lateral inflow from the floodplain to the main channel q^t_{fpm} are calculated by multiplying the absolute value of the depth-averaged fluctuation of the lateral velocity component $\left|\overline{v'}\right|$ with the interface area per unit length ($H - h_i$), where H is the flow depth in the main channel and a h_i is the depth of the main channel on the side of the floodplain i (Figure 1 a). It is assumed that the $\left|\overline{v'}\right|$ is proportional to the absolute value of the difference in streamwise velocities between two adjacent subsections $\left|U_{mc} - U_{fp}\right|$ [2]. Thus, the expression for the lateral turbulent momentum flux reads:

$$q^t_{mfp} = q^t_{fpm} = \left|\overline{v'}\right|(H - h_i) = \psi^t \left|U_{mc} - U_{fp}\right|(H - h_i) \tag{20}$$

where ψ^t is the proportionality factor. Since the turbulence momentum flux oscillates, Bousmar and Zech assume that it is equal to its doubled value through the interface between the two subsections [2].

Modelling of the exchange discharge due to change in geometry

One of the main parameters that affect floodplain conveyance is the width of the floodplain. Thus, the conveyance of the floodplain changes with the change in its width. It increases when it is widening and it reduces when it is narrowing. The change in conveyance forces a "geometrical transfer" discharge through the interface and results in the change in the discharge distribution between the main channel and floodplains along the course of the CCh. The "geometrical transfer" discharge from the main channel to the floodplain due to its widening is denoted by q^g_{mfp}, and that from the floodplain to the main channel due to its narrowing, by q^g_{fpm}. The possible layouts of the CCh and the corresponding directions of the "geometrical transfer" are presented in Figure 14.

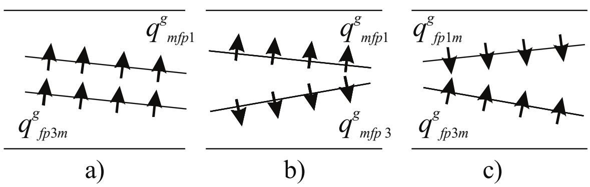

Figure 14. Possible layouts of the non-prismatic CCh: a) simultaneous widening of one, and narrowing of the other floodplain, with no change in the main channel width; b) simultaneous widening of both floodplains at the expense of narrowing of the main channel; and c) widening of the main channel at the expense of simultaneous narrowing of both floodplains [4]

For the case of increasing floodplain conveyance, the two "geometrical transfer" discharges are defined as:

$$q^g_{fpm} = 0 \quad \wedge \quad q^g_{mfp} = \frac{\mathrm{d}Q_{fp}}{\mathrm{d}x} = \frac{\mathrm{d}K_{fp}}{\mathrm{d}x} S^{1/2}_{f,fp} \tag{21}$$

and for the case of the decreasing floodplain conveyance, as:

$$q^{g}_{fpm} = -\frac{\mathrm{d}Q_{fp}}{\mathrm{d}x} = \frac{\mathrm{d}K_{fp}}{\mathrm{d}x} S^{1/2}_{f,fp} \qquad \wedge \qquad q^{g}_{mfp} = 0 \tag{22}$$

It is noted that the variation in the friction slope on the floodplain $S_{f,fp}$ due to change in its conveyance is neglected on the interval where the change in the conveyance is evaluated [5]. These expressions are generalised by introducing the κ parameter which indicates the flow direction with respect to the unit normal vector of the interface, and the proportionality factor ψ^g, which implicitly takes into account the aforementioned variation in the friction slope on the floodplain $S_{f,fp}$ due to change in its conveyance [2] [3] [5]:

$$q^{g}_{fpm} = \psi^{g} \kappa_{fpm} \frac{\mathrm{d}K_{fp}}{\mathrm{d}x} S^{1/2}_{f,fp} \qquad \wedge \qquad q^{g}_{mfp} = \psi^{g} \kappa_{mfp} \frac{\mathrm{d}K_{fp}}{\mathrm{d}x} S^{1/2}_{f,fp} \tag{23}$$

where

$$\kappa_{fpm} = \begin{cases} 0, & \dfrac{\mathrm{d}K_{fp}}{\mathrm{d}x} > 0 \\ -1, & \dfrac{\mathrm{d}K_{fp}}{\mathrm{d}x} < 0 \end{cases} \qquad \wedge \qquad \kappa_{mfp} = \begin{cases} 1, & \dfrac{\mathrm{d}K_{fp}}{\mathrm{d}x} > 0 \\ 0, & \dfrac{\mathrm{d}K_{fp}}{\mathrm{d}x} < 0 \end{cases} \tag{24}$$

The κ-value of 1 (κ = 1) indicates that the flow direction coincides with the unit normal vector of the interface, i.e. that the water outflows from the main channel to the floodplains. Conversely, κ = –1 shows that the flow is in the opposite direction of the unit normal vector of the interface and that the water withdraws from the floodplain to the main channel. Finally, κ = 0 implies that the considered subsection receives the water from the adjacent one.

EDM application

The EDM model is equally applicable to: 1. the estimation of the discharge in a compound channel based on the recorded flood marks for the purpose of estimation of the stage-discharge curve; and 2. the estimation of the slope of the energy grade line necessary for water level computations, when the water stage and the discharge are known. The following data are necessary for the estimation of discharge: 1. cross-sectional geometry; 2. the mean bottom slope S_0; 3. an estimation of the Manning roughness coefficient in all subsections of the CCh; and 4. the recorded flood mark(s). The estimation of the energy grade line slope, on the other hand, requires: 1. cross-sectional geometry; 2. the recorded flood mark(s); 3. the flood discharge; and 4. an estimation of the Manning roughness coefficient in all subsections of the CCh.

The two problems are solved using Manning's equation, Eq. 19, and the definition of the ratio χ_i. The discharge in the subsection i is calculated from:

$$Q_i = A_i U_i = \frac{A_i R_i^{2/3}}{n_i} S_{f,i}^{1/2} = K_i S_{f,i}^{1/2} = K_i \left(\frac{S_e}{1+\chi_i} \right)^{1/2} \tag{25}$$

and the mean velocity from:

$$V_i = \frac{R_i^{2/3}}{n_i} \left(\frac{S_e}{1+\chi_i} \right)^{1/2} \tag{26}$$

Expressions for χ_i, $i = 1, 2, 3$ can be derived from (19), (20) and (23). They read:

the left floodplain

$$\chi_1 = \frac{1}{gA_1} \left[\psi^t (H-h_1) \left(\frac{R_2^{2/3}}{n_2} \left(\frac{1+\chi_1}{1+\chi_2} \right)^{1/2} - \frac{R_1^{2/3}}{n_1} \right) + \psi^g \kappa_{21} \frac{dK_1}{dx} \right] \left[\frac{R_1^{2/3}}{n_1} - \frac{R_2^{2/3}}{n_2} \left(\frac{1+\chi_1}{1+\chi_2} \right)^{1/2} \right] \tag{27a}$$

the main channel

$$\begin{aligned} \chi_2 = {} & \frac{1}{gA_2} \left[\psi^t (H-h_1) \left(\frac{R_2^{2/3}}{n_2} \left(\frac{1+\chi_1}{1+\chi_2} \right)^{\frac{1}{2}} - \frac{R_1^{2/3}}{n_1} \right) + \psi^g \kappa_{12} \frac{dK_1}{dx} \right] \left[\frac{R_2^{2/3}}{n_2} \left(\frac{1+\chi_1}{1+\chi_2} \right)^{\frac{1}{2}} - \frac{R_1^{2/3}}{n_1} \right] \left(\frac{1+\chi_1}{1+\chi_2} \right) + \\ & + \frac{1}{gA_2} \left[\psi^t (H-h_3) \left(\frac{R_2^{2/3}}{n_2} \left(\frac{1+\chi_3}{1+\chi_2} \right)^{\frac{1}{2}} - \frac{R_3^{2/3}}{n_3} \right) + \psi^g \kappa_{32} \frac{dK_3}{dx} \right] \left[\frac{R_2^{2/3}}{n_2} \left(\frac{1+\chi_3}{1+\chi_2} \right)^{\frac{1}{2}} - \frac{R_3^{2/3}}{n_3} \right] \left(\frac{1+\chi_2}{1+\chi_3} \right) \end{aligned} \tag{27b}$$

the right floodplain

$$\chi_3 = \frac{1}{gA_3} \left[\psi^t (H-h_3) \left(\frac{R_2^{2/3}}{n_2} \left(\frac{1+\chi_3}{1+\chi_2} \right)^{1/2} - \frac{R_3^{2/3}}{n_3} \right) + \psi^g \kappa_{23} \frac{dK_3}{dx} \right] \left[\frac{R_3^{2/3}}{n_3} - \frac{R_2^{2/3}}{n_2} \left(\frac{1+\chi_3}{1+\chi_2} \right)^{1/2} \right] \tag{27c}$$

After introduction of three auxiliary variables:

$$X_i = (1+\chi_i)^{1/2} \tag{28}$$

the system of equations becomes:

$$X_1^2 - 1 = \frac{1}{gA_1} \left[\psi^t (H-h_1) \left(\frac{R_2^{2/3}}{n_2} \frac{X_1}{X_2} - \frac{R_1^{2/3}}{n_1} \right) + \psi^g \kappa_{21} \frac{dK_1}{dx} \right] \left[\frac{R_1^{2/3}}{n_1} - \frac{R_2^{2/3}}{n_2} \frac{X_1}{X_2} \right] \tag{29a}$$

$$X_2^2 - 1 = \frac{1}{gA_2}\left[\psi^t\left(H-h_1\right)\left(\frac{R_2^{2/3}}{n_2}\frac{X_1}{X_2}-\frac{R_1^{2/3}}{n_1}\right)+\psi^g\kappa_{12}\frac{\mathrm{d}K_1}{\mathrm{d}x}\right]\left[\frac{R_2^{2/3}}{n_2}\frac{X_1}{X_2}-\frac{R_1^{2/3}}{n_1}\right]\left(\frac{X_1}{X_2}\right)^2 + \\ + \frac{1}{gA_2}\left[\psi^t\left(H-h_3\right)\left(\frac{R_2^{2/3}}{n_2}\frac{X_3}{X_2}-\frac{R_3^{2/3}}{n_3}\right)+\psi^g\kappa_{32}\frac{\mathrm{d}K_3}{\mathrm{d}x}\right]\left[\frac{R_2^{2/3}}{n_2}\frac{X_3}{X_2}-\frac{R_3^{2/3}}{n_3}\right]\left(\frac{X_3}{X_2}\right)^2 \tag{29b}$$

$$X_3^2 - 1 = \frac{1}{gA_3}\left[\psi^t\left(H-h_3\right)\left(\frac{R_2^{2/3}}{n_2}\frac{X_3}{X_2}-\frac{R_3^{2/3}}{n_3}\right)+\psi^g\kappa_{23}\frac{\mathrm{d}K_3}{\mathrm{d}x}\right]\left[\frac{R_3^{2/3}}{n_3}-\frac{R_2^{2/3}}{n_2}\frac{X_3}{X_2}\right] \tag{29c}$$

Knowing that the velocity in the main channel is greater than that on the floodplains, the system (29) must satisfy the following conditions:

$$0 < X_1 \le 1 \ \wedge \ 1 \le X_2 \ \wedge \ 0 < X_3 \le 1 \tag{30a}$$

$$\frac{1}{X_1}\frac{R_1^{2/3}}{n_1} \le \frac{1}{X_2}\frac{R_2^{2/3}}{n_2} \qquad \wedge \qquad \frac{1}{X_3}\frac{R_3^{2/3}}{n_3} \le \frac{1}{X_2}\frac{R_2^{2/3}}{n_2} \tag{30b}$$

With these limitations, (29a) and (29c) can be considered quadratic equations in X_1 and X_3. For practical evaluation, only positive roots, which satisfy (30b) are taken:

$$\frac{X_1}{X_2} = \frac{1}{2}\left\{\left(2\frac{\psi^t\left(H-h_1\right)}{gA_1}\frac{R_1^{2/3}}{n_1}\frac{R_2^{2/3}}{n_2} - \frac{\psi^g\kappa_{21}\frac{\mathrm{d}K_1}{\mathrm{d}x}}{gA_1}\frac{R_2^{2/3}}{n_2}\right) + \left[\left(4\frac{\psi^t\left(H-h_1\right)}{gA_1} + \left(\frac{\psi^g\kappa_{21}\frac{\mathrm{d}K_1}{\mathrm{d}x}}{gA_1}\right)^2\right)\left(\frac{R_2^{2/3}}{n_2}\right)^2 + \right.\right. \\ \left.\left. + 4X_2^2\left(1 - \frac{\psi^t\left(H-h_1\right)}{gA_1}\left(\frac{R_1^{2/3}}{n_1}\right)^2 + \frac{\psi^g\kappa_{21}\frac{\mathrm{d}K_1}{\mathrm{d}x}}{gA_1}\frac{R_1^{2/3}}{n_1}\right)\right]^{\frac{1}{2}}\right\}\left[X_2^2 + \frac{\psi^t\left(H-h_1\right)}{gA_1}\left(\frac{R_2^{2/3}}{n_2}\right)^2\right]^{-1} \tag{31a}$$

$$\frac{X_3}{X_2} = \frac{1}{2}\left\{\left(2\frac{\psi^t\left(H-h_3\right)}{gA_3}\frac{R_3^{2/3}}{n_3}\frac{R_2^{2/3}}{n_2} - \frac{\psi^g\kappa_{23}\frac{\mathrm{d}K_3}{\mathrm{d}x}}{gA_3}\frac{R_2^{2/3}}{n_2}\right) + \left[\left(4\frac{\psi^t\left(H-h_3\right)}{gA_3} + \left(\frac{\psi^g\kappa_{23}\frac{\mathrm{d}K_3}{\mathrm{d}x}}{gA_3}\right)^2\right)\left(\frac{R_2^{2/3}}{n_2}\right)^2 + \right.\right. \\ \left.\left. + 4X_2^2\left(1 - \frac{\psi^t\left(H-h_3\right)}{gA_3}\left(\frac{R_3^{2/3}}{n_3}\right)^2 + \frac{\psi^g\kappa_{23}\frac{\mathrm{d}K_3}{\mathrm{d}x}}{gA_3}\frac{R_3^{2/3}}{n_3}\right)\right]^{\frac{1}{2}}\right\}\left[X_2^2 + \frac{\psi^t\left(H-h_3\right)}{gA_3}\left(\frac{R_2^{2/3}}{n_2}\right)^2\right]^{-1} \tag{31b}$$

After substitution of (31a) and (31b) into (29b) a single, non-linear equation in X_2 is obtained:

$$F\left(\frac{X_1}{X_2}, \frac{X_3}{X_2}, X_2\right) = F(X_2) = 0 \tag{32}$$

The equation is solved using the Newton-Raphson method. The remaining unknowns X_1 and X_3 are then calculated from (31a) and (31b). Consequently, three χ_i-ratio values are found from (28) and the discharge distribution between the subsections or the energy grade line slope can be determined. It is worth mentioning that the ratio χ_i is exclusively a function of the channel geometry and the roughness of subsections, which makes this method attractive for solving these practical engineering problems related to floods.

Total flood discharge is estimated from:

$$Q = \sum_i Q_i = \sum_i K_i \left(\frac{S_e}{1+\chi_i} \right)^{1/2} = \sum_i \left(\frac{K_i}{\left(1+\chi_i\right)^{1/2}} \right) S_e^{\ 1/2} \tag{33}$$

Since field measurements during floods are difficult and dangerous, the estimation is still based on an unrealistic and simplified assumption that the flow is uniform, i.e. that $S_e = S_0$. As it can be noticed, the EDM method makes use of corrected subsection conveyances:

$$K_i^* = \frac{K_i}{(1+\chi_i)^{1/2}},\ i = 1, 2, 3 \tag{34}$$

If, on the other hand, an energy grade line slope is needed for the water profile computations, it should be estimated based on the known water stage and total discharge values. In this case, the global ratio $\chi = S_{mot} / S_f$ (for the whole cross-section) is calculated based on the subsection ratios χ_i and conveyances K_i:

$$\chi = \left(\frac{\sum_i K_i}{\sum_i \left(K_i / \left(1+\chi_i\right)^{1/2} \right)} \right)^2 - 1 \tag{35}$$

and the S_e is then calculated from:

$$S_e = S_f + S_{mot} = S_f \left(1+\chi\right) = \left(\frac{Q}{\sum_i K_i} \right)^2 \left(1+\chi\right) \tag{36}$$

Here, S_{mot} is a global momentum transfer for the cross-section.

Independent subsections method (ISM)

In contrast to EDM, where a single water level value for the cross-section is calculated, the water surface profile in the ISM is estimated within each subsection. Moreover, the additional loss due to momentum transfer between adjacent subsections is explicitly divided into two terms – one that refers to the apparent shear stress (τ_{ij}) acting on the interface between subsections (which is responsible for the momentum transfer due to turbulence diffusion) and the other, which refers to the lateral mass exchange by the lateral discharge per unit length (q_{in} and/or q_{out}). In ISM, Eq. 15 for the steady flow transforms to:

$$S_{f,i} = S_0 - \frac{\mathrm{d}h_i}{\mathrm{d}x} \pm \frac{\tau_{ij} h_{if}}{\rho g A_i} - \frac{1}{gA_i}\frac{\mathrm{d}}{\mathrm{d}x}\left(A_i U_i^2\right) + \frac{\left(U_{in} q_{in} - U_{out} q_{out}\right)}{gA_i}, \; i = 1, 2, 3 \qquad (37)$$

where h_i is the flow depth in the subsection i, h_{if} is the flow depth at the interface between adjacent subsections, U_{in} and U_{out} are subsection streamwise velocities with which the lateral mass discharge enters and leaves the subsection, respectively. Other variables are the same as in (15).

The mass conservation equation for each subsection reads:

$$\frac{\mathrm{d}A_i U_i}{\mathrm{d}x} = q_{in} - q_{out}, \; i = 1, 2, 3 \qquad (38)$$

In the CCh with three subsections (Figure 1 a), there are only two lateral mass discharges: the one between the left floodplain and the main channel q_{lm} and the other, between the right floodplain and the main channel q_{rm}. The lateral discharge is positive when mass leaves the floodplain, and negative when it enters the floodplain. Thus, the following is valid: 1. for the left floodplain $q_{out} = q_{lm}$ and $q_{in} = 0$; 2. for the right floodplain $q_{out} = q_{rm}$ and $q_{in} = 0$ and for the main channel $q_{out} = 0$ and $q_{in} = q_{lm} + q_{rm}$. Eq. 38 can be written now for each subsection:

the left floodplain

$$\frac{\mathrm{d}Q_l}{\mathrm{d}x} = -q_{lm} \qquad (39)$$

the right floodplain

$$\frac{\mathrm{d}Q_r}{\mathrm{d}x} = -q_{rm} \qquad (40)$$

the main channel

$$\frac{\mathrm{d}Q_m}{\mathrm{d}x} = q_{lm} + q_{rm} \qquad (41)$$

The mass conservation equation for the CCh cross-section as a whole is reached by combining (39)–(41) into a single one:

$$\frac{\mathrm{d}Q_m}{\mathrm{d}x} + \frac{\mathrm{d}Q_l}{\mathrm{d}x} + \frac{\mathrm{d}Q_r}{\mathrm{d}x} = 0 \qquad (42)$$

Momentum equations for the three subsections are derived from (37) and (38) in the form similar to that for simple-channel non-uniform flow:

the left floodplain

$$\left(1 - \frac{U_l^2}{gh_l}\right)\frac{\mathrm{d}h_l}{\mathrm{d}x} = S_0 - S_{fl} + \frac{U_l^2}{gB_l}\frac{\mathrm{d}B_l}{\mathrm{d}x} + \frac{\tau_{lm} h_l}{\rho g A_l} + \frac{q_{lm}\left(2U_l - U_{if,l}\right)}{gA_l} \qquad (43)$$

the right floodplain

$$\left(1-\frac{U_r^2}{gh_r}\right)\frac{\mathrm{d}h_r}{\mathrm{d}x} = S_0 - S_{fr} + \frac{U_r^2}{gB_r}\frac{\mathrm{d}B_r}{\mathrm{d}x} + \frac{\tau_{rm}h_r}{\rho g A_r} + \frac{q_{rm}\left(2U_r - U_{if,r}\right)}{gA_r} \tag{44}$$

the main channel

$$\left(1-\frac{U_m^2}{gh_m}\right)\frac{\mathrm{d}h_m}{\mathrm{d}x} = S_0 - S_{fm} + \frac{U_m^2}{gB_m}\frac{\mathrm{d}B_m}{\mathrm{d}x} - \frac{\tau_{lm}h_l}{\rho g A_m} - \frac{\tau_{rm}h_r}{\rho g A_m} - \\ - \frac{q_{lm}\left(2U_m - U_{if,l}\right)}{gA_m} - \frac{q_{rm}\left(2U_m - U_{if,r}\right)}{gA_m} \tag{45}$$

The width of the subsection is denoted by B_i. It is assumed that all subsections are rectangular. Shear stresses at interfaces τ_{lm} and τ_{rm} are modelled by:

$$\left|\tau_{lm}\right| = \rho\psi^t (U_{mc} - U_l)^2 \text{ and } \left|\tau_{rm}\right| = \rho\psi^t (U_{mc} - U_r)^2 \tag{46}$$

where ψ^t is, again, the model parameter. Streamwise velocities at the interface between the main channel and the left and right floodplains are denoted by $U_{if,l}$ and $U_{if,r}$, respectively. Proust et al. [12] distinguished three possible cases for defining interface velocities:

the prismatic CCh and transfer of mass which occurs from subsection *i* towards subsection *j*:

$$U_{if} = U_i \tag{47}$$

the non-prismatic CCh and constant total channel width:

$$U_{if} = U_i \qquad \text{if} \qquad \mathrm{d}B_i/\mathrm{d}x < 0 \tag{48}$$

$$U_{if} = U_j \qquad \text{if} \qquad \mathrm{d}B_i/\mathrm{d}x > 0 \tag{49}$$

the non-prismatic CCh with variable total channel width:

$$U_{if,l} = \varphi_l U_l + (1-\varphi_l)U_m \qquad \text{and} \qquad U_{if,r} = \varphi_r U_r + (1-\varphi_r)U_m \tag{50}$$

Knowing that $E_i = Z_i + U_i^2 / 2g$ is the subsection total head, the Z_i being the water level in subsection *i*, Eq. 37 can be written as follows:

$$S_{e,i} = -\frac{\mathrm{d}E_i}{\mathrm{d}x} = S_{f,i} \pm \frac{\tau_{ij}h_{if}}{\rho g A_i} + \frac{q_{in}(U_i - U_{in}) + q_{out}(U_{out} - U_i)}{gA_i} = \\ = S_{f,i} + S_{td,i} + S_{m,i} \tag{51}$$

With this notation, knowing that the second term in the bracket on the left hand side is Froude number, the analogy with equations for the simple-channel non-uniform flow becomes more obvious:

$$\left(1-\underbrace{\frac{U_l^2}{gh_l}}_{\mathrm{Fr}_i}\right)\frac{\mathrm{d}h_l}{\mathrm{d}x}=S_0-\underbrace{S_{fl}+\frac{U_l^2}{gB_l}\frac{\mathrm{d}B_l}{\mathrm{d}x}+\frac{\tau_{lm}h_l}{\rho gA_l}+\frac{q_{lm}\left(2U_l-U_{if,l}\right)}{gA_l}}_{S_{e,i}} \tag{52}$$

$$\left(1-\mathrm{Fr}_i\right)\frac{\mathrm{d}h_l}{\mathrm{d}x}=S_0-S_{e,i}$$

The system of three mass conservation and three momentum conservation equations together with the four closure equations is solved iteratively using finite differences.

Comparative analysis of traditional and new, improved models and the assessment of their performance

The two models from the previous section were tested and compared against the data from the FCF (Flood Channel Facility) made in HR Wallingford (Figure 15). This is a straight two-stage channel of trapezoidal cross-section in both the main channel and floodplains. The channel is 56 m long and 10 m wide.

The longitudinal slope of the channel is S_0 = 1.027%. The main channel is made of concrete, and floodplains are made of Plexiglas. Channel dimensions from Figure 1 a, including bank slopes are given in Table 1. Experimental series with smooth and rough floodplains were used for calibration and comparison of the two models (Table 1). The first two cases (series no. 2 and 3) with smooth floodplains were used to study sensitivity of models to changes in CCh width.

The first and the third case (series no. 2 and 6) were used to test the model in the absence or complete exclusion of one floodplain, i.e. symmetrical vs. asymmetrical CCh results were compared. Finally, the first and the fourth case (series no. 2 and 7) were used to assess the models' ability to estimate the stage-discharge curve in a real case, i.e. when floodplains are rough and when it increases with the flow depth (this would correspond to the case of emergent vegetation on the floodplains).

In cases with smooth floodplains, the estimated value of Manning's coefficient of n = 0.01 $\mathrm{m}^{-1/3}\mathrm{s}$ was used, while the variation of the Manning's coefficient value with the depth for the rough floodplains was defined based on the experimental data [1]. The flow in all experimental series was uniform. Eight overbank depths were considered in each series.

Figure 15. Flood channel Facility in HR Wallingford [8]

Table 1. Geometry of FCF for different compound channel layouts [9]

Series No. (layout)	**B** [m]	**b** [m]	**B/b** [/]	m_{mc} [/]	**Floodplain roughness**
2	6.3	1.5	4.20	1	no
3	3.3	1.5	2.20	1	no
6	6.3	1.5	4.20	1	no
7	6.3	1.5	4.20	1	yes

Stage-discharge curves for different compound channel geometries

Symmetrical compound channels

Stage-discharge curves calculated using two presented methods (EDM and ISM) and two traditional methods (SCM and DCM) are compared to measured ones in Figure 16 a. Values of the ψ^t parameter were adjusted to achieve the best agreement with measurements. The value of the parameter $\psi^g = 0$, since the channel is prismatic. The optimal value of ψ^t parameter in EDM depends on the overall width of the CCh. In narrower channels ($B / b = 2.20$) it is greater ($\psi^t = 0.10$) than in wider channels ($\psi^t = 0.05$). In both cases, discrepancies from the measured values are within the measurement error – they are less than 5% (Table 2). On the other hand, the optimal value of the ψ^t parameter does not depend on the overall CCh width – it is 0.065. However, the maximal discrepancy exceeds 5% at low floodplain depths when $B / b = 2.20$ and at high floodplain depths when $B / b = 4.20$. The total discharge is over predicted by 8% in the former case, while in the latter case, the percentage is even greater – 13.6% (Table 2). In the remaining part of the stage-discharge curve, discharges predicted by ISM are slightly greater than those predicted by EDM (the differences amount to 4%). Traditional methods produce much greater discrepancies from the measured discharge values – SCM at low floodplain depths, when there is pronounced transfer of momentum between the main channel and the floodplain, under estimates discharge values up to 46%, while the DCM overestimate discharges by approximately 10%.

It is interesting to note that the two traditional methods produce much lower discrepancies at high relative floodplain depths $(H - h) / h > 0.31$ – for DCM they are below 7% and for SCM, they are below 5%. This amelioration of traditional methods' performance can be explained by the fact that the hydraulic conditions in the CCh cross section gradually tend to become uniform again at high floodplain depths. This justifies the application of traditional methods in discharge estimation only at very high relative floodplain depths.

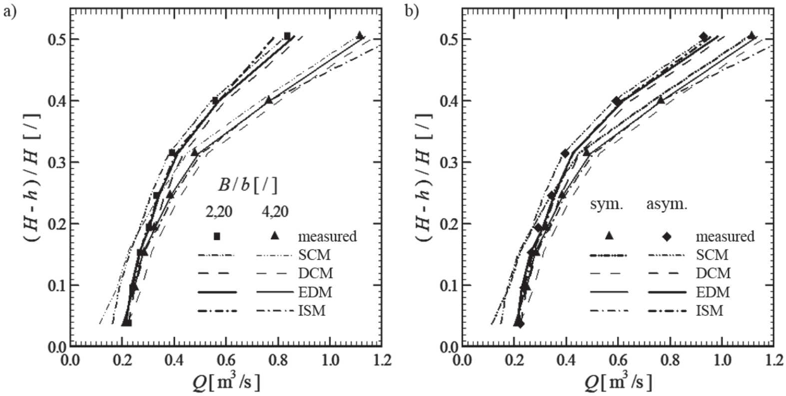

Figure 16. Comparison of calculated and measured stage-discharge curves for the entire cross-section: a) effect of floodplain width; b) effect of floodplain asymmetry (B / b = 4.20) [9]

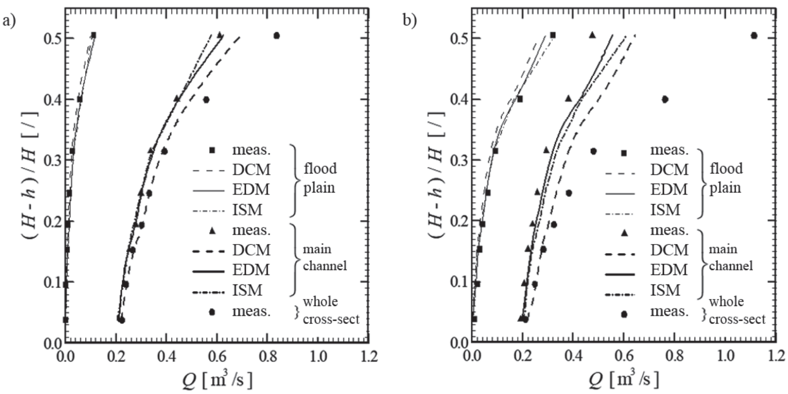

Figure 17. Comparison of calculated and measured discharge distributions between main channel and floodplain. Effect of floodplain width: a) B / b = 2.20; b) B / b = 4.20 [9]

Advantages of new methods in stage-discharge curve estimation become even more obvious when the discharge distribution between the main channel and floodplains is considered (Figure 17). This is particularly highlighted when it comes to the analysis of sediment transport and related processes on floodplains.

The estimation by the EDM and ISM is much better than that by the DCM. In narrower CChs, where the momentum transfer is more pronounced, the EDM performs slightly better than the ISM both in the main channel and floodplains (Table 2). Discrepancies for the DCM are 2.0–2.5 greater than those for the EDM.

Asymmetrical compound channels

Stage-discharge curves for symmetrical and asymmetrical CChs are compared in Figure 16 b. Both the plotted stage-discharge curves and the data from Table 2 confirm that both the EDM and the ISM satisfactorily estimate total discharge in the asymmetrical CCh – discrepancies range from 3 to 8%.

However, discrepancies for the DCM are 1.5 to 4.0 times greater than those for EDM and ISM. Results for the SCM show similar behaviour as for the symmetrical CChs – for $(H - h) / h < 0.31$ values of the discharge are considerably underestimated (20–30%), whereas at high relative floodplain depths they reduce to only 2%.

As far as the discharge distribution between the main channel and floodplains is concerned, new methods perform well, with the note the ISM now gives slightly better results than the EDM (Table 2). In this case, discrepancies for the DCM are 2.5–5.0 times greater than those for EDM.

Table 2. Ranges of relative discrepancies between calculated and measured discharges for the whole cross-section, main channel and floodplain [9]

	Series No.			
	2	3	6	7
Method	**Whole cross-section**			
SCM	–46.0 ÷ –1.0	–27.8 ÷ –0.7	–33.6 ÷ 1.8	–49.5 ÷ –25.5
DCM	3.5 ÷ 11.1	–0.5 ÷ 11.0	0.4 ÷ 14.2	2.4 ÷ 59.0
EDM	–4.4 ÷ 2.6	–5.1 ÷ 5.3	–5.5 ÷ 7.4	–4.5 ÷ 3.7
ISM	–48 ÷ 13,6	-7,9 ÷ 3.5	–3.3 ÷ 7.9	–4.6 ÷ 5.6
	Main channel			
DCM	13.0 ÷ 35.6	–0.3 ÷ 14.5	4.0 ÷ 20.4	8.0 ÷ 105.9
EDM	3.1 ÷ 16.8	–5.4 ÷ 4.1	–5.4 ÷ 8.8	0.8 ÷ 7.2
ISM	4.8 ÷ 28.6	–7.5 ÷ 1.4	–2.3 ÷ 7.6	1.5 ÷ 9.5
	Floodplain			
DCM	–47.6 ÷ –17.5	–24.5 ÷ –9.7	–11.0 ÷ 0.4	–79.4 ÷ –20.9
EDM	–28.6 ÷ –7.5	3.7 ÷ 33.3	0.4 ÷ 54.8	–69.7 ÷ –2.0
ISM	–52.4 ÷ 2.2	–6.8 ÷ 57.2	–3.7 ÷ 34.9	–71.1 ÷ –1.6

Stage-discharge curves for different floodplain roughness

The estimation of the stage-discharge curve with new methods for the case with rough floodplains (Figure 18) required adjustment of the ψ^t parameter values for a second time. It was found that the best agreement with measurements in the EDM was achieved for ψ^t parameter values between 0.05 and 0.10, while the optimal value for the ISM was the same as for CChs with smooth floodplains, i.e. $\psi^t = 0.065$. When the floodplain is rough, velocity gradients between the main channel and the floodplain is greater, and the advantages of new methods become even more obvious. Discrepancies do not exceed 6% (Table 2). The SCM underestimates total discharge by 25–50%, while the overestimate by DCM increases with the floodplain flow depth from 2.4 to 60%. If one neglects high discrepancies at very low floodplain depths (around 70%), when the measurement error is comparably high, it can be said that both the EDM and the ISM successfully assess the distribution between the main channel and floodplains – discrepancies for the main channel are less than 7.5% for the EDM and less than 9.5% for the ISM. On floodplains where the floodplain discharge does not exceed 20% of the total discharge, disagreement is greater, but it can be attributed to higher uncertainties in measured variables that result from difficulties in velocity measurements at the interface between the main channel and the floodplain.

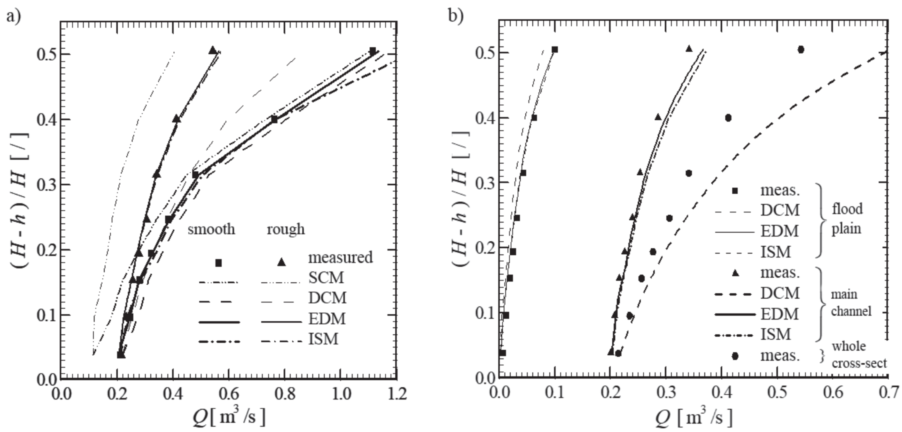

Figure 18. Comparison of calculated and measured stage-discharge curves. Effect of floodplain roughness (B / b = 4.20): a) total discharge; b) discharge distributions between main channel and floodplain [9]

References

[1] Ackers P (1993). Flow Formulae for Straight Two-stage Channels. J Hydr Res. 31(4):509–531.

[2] Bousmar D, Zech Y (1999). Momentum Transfer for Practical Flow Computation in Compound Channels. J Hydr Eng. 125(7):696706. DOI: https://doi.org/10.1061/(ASCE)0733-9429(1999)125:7(696)

[3] Bousmar D, Wilkin N, Jacquemart J-H, Zech Y (2004). Overbank Flow in Symmetrically Narrowing Floodplains. J Hydr Eng. 130(4):305–312. DOI: https://doi.org/10.1061/(ASCE)0733-9429(2004)130:4(305)

[4] Đorđević D, Stojnić I, Muhić F (2015). Prikaz modela linijskog tečenja u koritu za veliku vodu zasnovanog na razmeni količine kretanja između glavnog korita i plavnih površina. Vodoprivreda 47(273–275):79–91.

[5] Đorđević D, Stojnić I, Rosić N (2017). Water Profile Computations in Non-prismatic Compound Channels with Simple Cross-sectional Geometry Using Exchange Discharge Model. Vodoprivreda 49(282–284):167–179.

[6] Ghisalberti M, Nepf MH (2002). Mixing Layers and Coherent Structures in Vegetated Aquatic Flows. J Geoph Res. 107(C2):3-1–3-11. DOI: https://doi.org/10.1029/2001JC000871

[7] Gunawan B (2010). A Study of Flow Structures in a Two-stage Channel Using Field Data, a Physical Model and Numerical Modelling. PhD thesis, University of Birmingham. 322p.
[8] Knight DW, Aya S, Ikeda S, Nezu I, Shiono K (2009). Flow Structure. In: Ikeda S, McEwan IK editors. Flow and Sediment Transport in Compound Channels. London: CRC Press. 342 p.
[9] Мухић Ф, Станић Ф, Стојнић И, Ђорђевић Д (2015). Application of EDM and ISM Methods in Estimation of Stage-discharge Curve in a Compound Channel. 17th SAHI and SAH Conference. p. 125–135.
[10] Nepf MN (2012). Hydrodynamics of Vegetated Channels. J Hydr Res. 50(3):262–279. DOI: https://doi.org/10.1080/00221686.2012.696559
[11] Nikora V, Ballio F, Coleman S, Pokrajac D (2013). Spatially Averaged Flows over Mobile Rough Beds: Definitions, Averaging Theorems, and Conservation Equations. J Hydr Eng. 139(8):803–811, DOI: https://doi.org/10.1061/(ASCE)HY.1943-7900.0000738
[12] Proust S, Bousmar D, Riviere N, Paquier A, Zech Y (2009). Non-uniform flow in compound channel: A 1-D method for assessing water level and discharge distribution. Water Resour Res. 45(12). DOI: https://doi.org/10.1029/2009WR008202
[13] Radojković M (1980). Matematički model kretanja vode u otvorenim tokovima složenog preseka. Doktorska disertacija, Građevinski fakultet, Beograd.
[14] Стојнић И, Мухић Ф, Ђорђевић Д (2015). Study of the Influence of Channel Geometry and Hydraulic Resistance on Flow Characteristics in Compound Channels. 17th SAHI and SAH Conference. p. 114–124.
[15] Valentine EM, Ikeda S, Knight DW, McEwan IK, Myers WRC, Pender G, Tsujimoto T, Willetts BB, Wormleaton PR (2009). Sediment Processes. In: Ikeda S, McEwan IK editors. Flow and Sediment Transport in Compound Channels. London: CRC Press. p. 342.
[16] Wormleaton PR, Merrett DJ (1990). An Improved Method of Calculation for Steady Uniform Flow in Prismatic Main Channel/Flood Plain Sections. J Hydr Res. 28(2):157–174. DOI: https://doi.org/10.1080/00221689009499084